Journal of Communications Technology and Electronics, Vol. 50, No. 6, 2005, pp. 622–637. Translated from Radiotekhnika i Elektronika, Vol. 50, No. 6, 2005, pp. 678–696.

RADIO PHENOMENA IN SOLIDS AND PLASMA

Silicon-on-Sapphire Structures as a Material for Piezoresistive Mechanical Transducers

V. M. Stuchebnikov

Received November 1, 2004

Abstract—An overview is presented of silicon-on-sapphire (SOS) structures in relation to their use as piezoresistive sensing elements in mechanical transducers. The status of and trends in the development of SOS pressure transducers are discussed.

INTRODUCTION

Silicon-on-sapphire (SOS) heteroepitaxial structures [1] captured the attention of both semiconductor-materials experts and IC designers immediately after they were first fabricated in the mid-1960s. Since sapphire is an excellent insulator, SOS structures were seen as a way of increasing the speed of complementary metal–oxide semiconductor (CMOS) circuits. They were also expected to provide high-radiation- resistant ICs. These expectations gave impetus to extensive research on SOS growth, structure, and electrical properties [1]. However, subsequent progress in bulk-silicon technology led to a dramatic increase in the speed of CMOS circuits while decreasing their cost to a level well below that of SOS structures. As a result, SOS ICs are mainly used where radiation hardness is required; they currently have no serious competitors in this field [2, 3]. SOS ICs are also employed in optoelectronics [4].

There is yet another field of application, which emerged shortly after SOS technology came into focus: piezoresistive transducers of mechanical parameters (force, pressure, etc.) [5, 6]. Initiated in the USSR, this application was first developed at NIITeplopribor (Moscow) and the Research Institute of Measurement Technology (Korolev) and then at several enterprises such as the Research and Production Complex "Ulyanovsk Center of Microelectronics and Automation" (NPK UZM, Ulyanovsk), the Industrial Group "Microelectronic Sensors" (IG MIDA, Ulyanovsk), IG Metran (Chelyabinsk), etc. Piezoresistive sensing elements based on SOS structures were employed in mass-produced devices including the Kristall pressure transducer [7], the Sapfir [8] and Sapfir-22 [9] measuring systems, and the MIDA series of pressure transducers [10].

As compared with well-known silicon sensing elements based on diffused or ion-implanted piezoresistors, SOS sensing elements have several advantages [11, 12]. First, SOS sensing elements do not use a *p*–*n* junction as silicon ones do to isolate the piezoresistors from the substrate; as a result, the breakdown voltage is raised by an order of magnitude and the operating temperature of sensing elements is made several times higher. Second, uniform doping of the SOS film allows one to easily control the characteristics of sensing elements and transducers. Third, a hard, insulating substrate opens additional possibilities for the improvement of sensing elements and transducers. Fourth, SOS structures (and also SOS sensing elements) have high radiation hardness. It is also important to note that SOS-transducer technology almost eliminates the need for a clean working environment. For the above reasons, using SOS structures in piezoresistive transducers has proven to be so successful that the technology has been implemented in an overwhelming majority of pressure transducers being produced in Russia [13–15]. This application of SOS structures has recently found acceptance abroad [16–18].

This paper is an overview concerned with SOS structures in relation to piezoresistive mechanical transducers, the performance of SOS pressure transducers and transmitters currently produced in Russia, and prospective developments in SOS piezoresistive sensors.

1. ELECTRICAL PROPERTIES OF SOS STRUCTURES

The SOS structure is a monocrystalline silicon film 0.1–5.0 μm thick grown on single-crystal sapphire (Al_2O_3), usually by silane pyrolysis [1]. As sapphire and silicon differ in crystal structure, a sapphire substrate must have an appropriate orientation in order for a single-crystal silicon film to grow [19]. The $Si(001)/Al_2O_3(1\bar{1}02)$ combination (Fig. 1) is the most suitable for piezoresistive sensing elements and the most useful for the electronics industry [20, 21]. As with silicon sensing elements, an SOS film should have *p*-type conduction with hole concentration *p* greater than 10^{18} cm^{-3} for the considered application.

The factors affecting the electrical properties of SOS films are the Al migration from the substrate during growth, film defects, and high thermal stress [1, 22, 23].

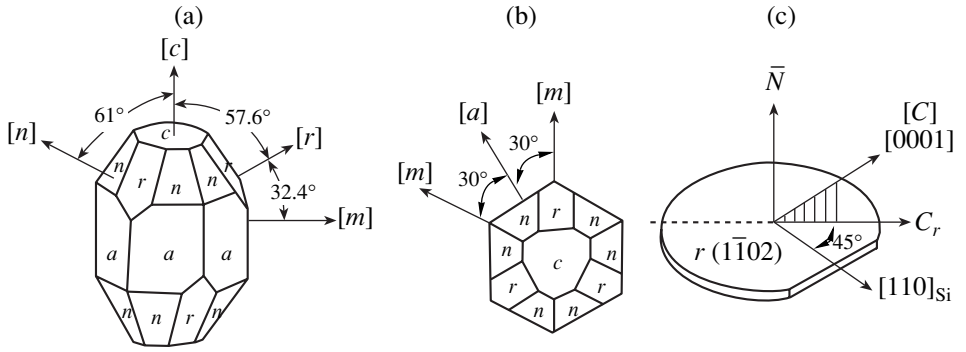

Fig. 1. (a, b) Crystallographic planes and directions in synthetic sapphire (α-Al_2O_3) and (c) crystallographic directions in an SOS structure made up of a Si(001) film on an $r(1\bar{1}02)$ sapphire substrate [21]. In panels (a, b), the three equivalent *r* planes have the indices $(01\bar{1}2)$, $(\bar{1}012)$, and $(1\bar{1}02)$, respectively. In panel (c), *N* is the substrate normal and C_r is the *C* axis of the sapphire projected on the *r* plane; the substrate is cut normal to the [110] direction of the silicon.

In silane pyrolysis the interaction between Al_2O_3 and the SiH_4–H_2 mixture results in migration of combined or free aluminum, a shallow acceptor that contaminates the growing SOS film, especially during the initial stage of growth. However, the influence of aluminum ($N_{Al} \sim 10^{15}$ cm^{-3}) is negligible in highly doped films.

SOS films show a high defect density, particularly near the interface, on account of lattice mismatch, misorientation of silicon nuclei during growth, and thermal-stress relaxation (Fig. 2). As a result, SOS films have a lower carrier mobility compared with bulk silicon (Fig. 3). On the other hand, the carrier mobility is almost independent of Si thickness *d* down to $d \sim 0.15$ μm (Fig. 4) in the case of high doping, implying an insignificant influence of defect scattering on the hole mobility. Thus, as with bulk silicon, the resistivity of a heavily doped *p*-SOS film is a function of hole concentration, provided that a well-established growth process has been performed (Fig. 5).

Since sapphire has a coefficient of thermal expansion almost twice as large as that of silicon (Fig. 6), SOS structures experience thermal stress that is high in magnitude and nonuniform over the thickness of the Si film and the substrate, *d* and *D*, respectively (Fig. 7). Mechanically, thermal stress is manifested in bending of the SOS structure; measurement of the curvature radius enables direct determination of mean thermal stress τ_0 in silicon [33], which was found to be $(4–6) \times 10^8$ Pa, as predicted. If the Si thickness is increased to a value such that $d/D > 0.4$, the substrate stress becomes so high that plastic deformation occurs in the sapphire in the temperature range 1100–900°C, the actual bending exceeding predictions [34]. Bending leads to an

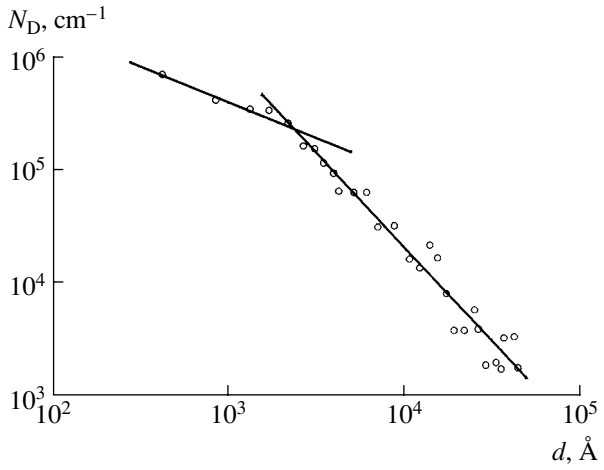

Fig. 2. Linear defect density vs. distance to the interface for an SOS film; $N_D \le 10^2$ cm^{-1} for $d \ge 4$ μm (the resolution limit of the method) [24].

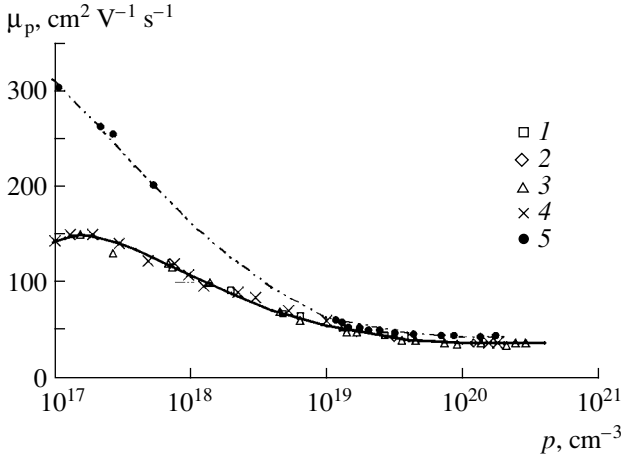

Fig. 3. Hole mobility vs. carrier density subject to Si thickness *d* in a *p*-SOS structure at room temperature [25]. The data points refer to (*1*) $d < 1$ μm, (*2*) 1 μm $\le d \le 2$ μm, (*3*) $d > 2$ μm, (*4*) $d = 2$ μm, and (*5*) bulk silicon. Data points *4* and *5* are borrowed from [26] and [27], respectively.

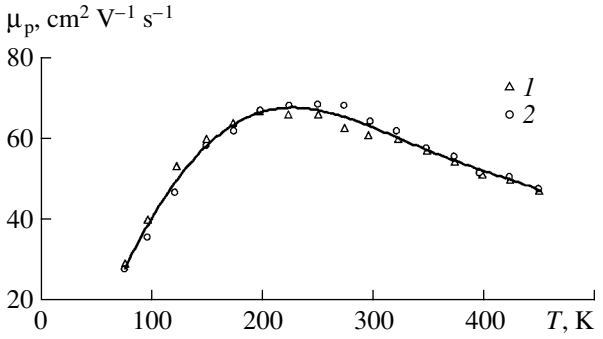

Fig. 4. Temperature dependence of hole mobility in an SOS film (*1*) 4.5 or (*2*) 0.15 μm thick; $p = 6.0 \times 10^{18}$ cm^{-3} and $\rho = 0.017$ Ω cm [25].

inhomogeneous SOS film and inaccurate photolithography, so a sufficiently thick substrate ($d/D < 0.01$) is required in order to produce a high-quality SOS structure. In general, thermal stress distorts the band structure of silicon and affects its electrical behavior [22]. However, the thermal stress in a thin continuous *p*-SOS film is virtually uniform and isotropic and thus has an insignificant influence on the hole mobility and, hence, resistivity. On the other hand, the thermal compressive stress in a *p*-SOS film changes the temperature coefficient of sensitivity of the piezoresistive sensing element as a result of the nonlinear nature of the piezoresistive effect [25]. Also note that the effect of thermal stress is especially strong in narrow silicon piezoresistors in the form of mesas (see below).

Experiments have shown that for a homogeneous, heavily doped *p*-SOS film the temperature dependence of resistivity $\rho(T)$ closely obeys an exponential relation:

$$\rho(T) = \rho_0 \exp(\alpha_\rho T), \tag{1}$$

where α_ρ is the differential temperature coefficient of resistivity for the silicon. This is constant over a wide temperature range at suitable doping levels [11].

2. PIEZORESISTIVE EFFECT IN *p*-SOS STRUCTURES

The piezoresistive effect in heavily doped *p*-SOS structures was investigated over the temperature range 4–800 K [11, 35–38]. The resistivity–strain relationship in an SOS film is written

$$\rho_i \approx \rho_0(1 + m_{ij}\varepsilon_j + m_{ijk}\varepsilon_j\varepsilon_k + m_{ijkl}\varepsilon_j\varepsilon_k\varepsilon_l), \quad i, j, k, l = 1, 2, \ldots 6, \tag{2}$$

where ρ_0 is the isotropic resistivity of unstrained silicon; ρ_i and ε_j are the resistivity and strain components, respectively; and m_{ij}, m_{ijk}, and m_{ijkl} are the first-, second-, and third-order elastoresistivity coefficients, respectively. According to Eq. (2) the resistivity is generally a nonlinear function of strain. The response of a

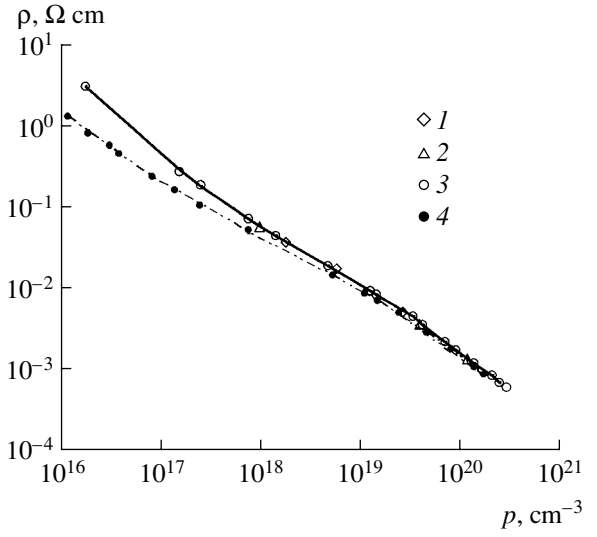

Fig. 5. Si resistivity vs. hole density subject to Si thickness *d* in a *p*-SOS structure at room temperature: (*1*) $d < 1$ μm, (*2*) 1 μm $\le d \le 2$ μm, and (*3*) $d > 2$ μm. Data points *4* refer to uniformly doped bulk silicon [28].

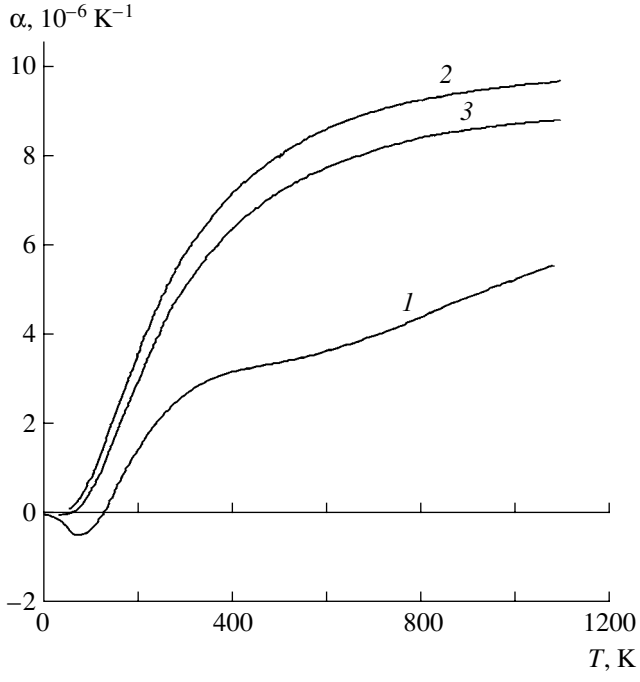

Fig. 6. Temperature dependence of the coefficients of linear thermal expansion for (*1*) silicon [29, 30] and (*2*, *3*) colorless sapphire; for the latter, directions (*2*) parallel and (*3*) perpendicular to the *C* axis are considered [31]. The temperature range is 6–1100 K.

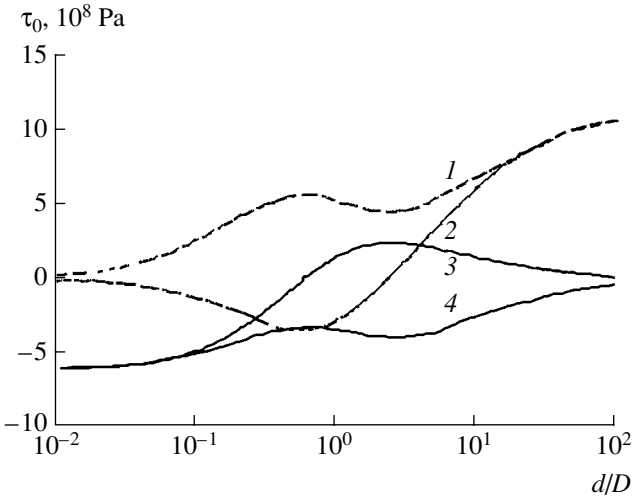

Fig. 7. Calculated thermal stress vs. silicon-to-sapphire thickness ratio [32]. The curves represent (*1*) the interface layer of sapphire, (*2*) the free sapphire surface, (*3*) the free silicon surface, and (*4*) the interface layer of silicon.

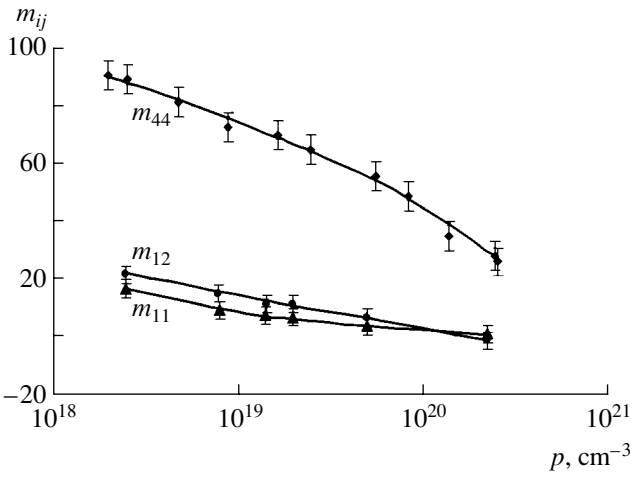

Fig. 8. Elastoresistivity components vs. hole density for a *p*-SOS structure at room temperature [37].

piezoresistor to strain is commonly measured by gage factor K defined by

$$\Delta R/R = K(T)\varepsilon = K^{(1)}(T)\varepsilon + K^{(2)}(T)\varepsilon^2 + K^{(3)}(T)\varepsilon^3, \quad (3)$$

where $\Delta R/R$ is the fractional change in resistance; ε is the characteristic strain (it varies as ε_j); and $K^{(1)}$, $K^{(2)}$, and $K^{(3)}$ are the first-, second-, and third-order gage factors (related to m_{ij}, m_{ijk}, and m_{ijkl}, respectively). Note that $K^{(2)}$ or $K^{(3)}$ is negligible if strain ε is parallel or perpendicular, respectively, to the piezoresistor axis; this applies to diffused *p*-Si piezoresistors in the <110> orientation on Si(001), as in Si sensing elements [39].

At room temperature, m_{11}, m_{12}, and m_{44} for a *p*-SOS film (Fig. 8) are close to those for bulk *p*-Si. This is not the case at low temperatures, mainly because of the thermal stress experienced by the film [36]. Unlike bulk silicon (let alone diffused silicon films), the measured variation of m_{44} with temperature closely obeys an exponential relation:

$$m_{44}(T) = m_{440}\exp(\alpha_m T), \quad (4)$$

the differential temperature coefficient of elastoresistivity, α_m, being constant over a wide temperature range at suitable hole concentrations (Fig. 9) [37].

In contrast to diffused silicon piezoresistors, $K^{(3)}$ in *p*-SOS is negligible at any orientation of strain relative to the piezoresistor axis. The respective values of $K^{(2)}$ for longitudinal and transverse strains are strongly temperature dependent, yet they are almost equal over the temperature range 4–800 K (Fig. 10) [38].

The fact that $\rho(T)$ and $m_{44}(T)$ can be approximated by exponential functions of temperature (see Eqs. (1) and (4)) is very important to the design of precision mechanical transducers. Consider widely used transducers having a Si(001) diaphragm sensing element with piezoresistors oriented along the ⟨100⟩ directions, located at the edge of the diaphragm, and arranged in a bridge. It has been shown that output U of the bridge is related to measured parameter M (e.g., pressure) as

$$U = I_E R_0 K_s m_{44} M \quad (5)$$

or as

$$U = U_E K_s m_{44} M \quad (6)$$

if the bridge is excited by a constant-current or con-

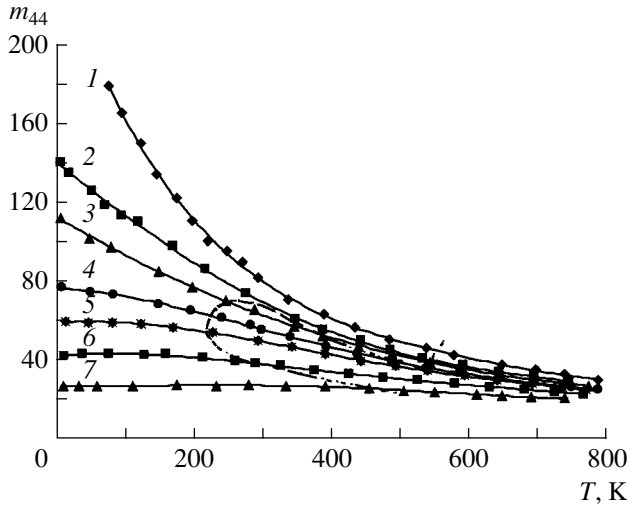

Fig. 9. Temperature dependence of m_{44} for a hole density of (*1*) 4.6×10^{18}, (*2*) 1.6×10^{19}, (*3*) 2.3×10^{19}, (*4*) 5.4×10^{19}, (*5*) 8.4×10^{19}, (*6*) 1.3×10^{20}, or (*7*) 2.3×10^{20} cm^{-3}. The dashed line marks the regions where Eq. (4) holds.

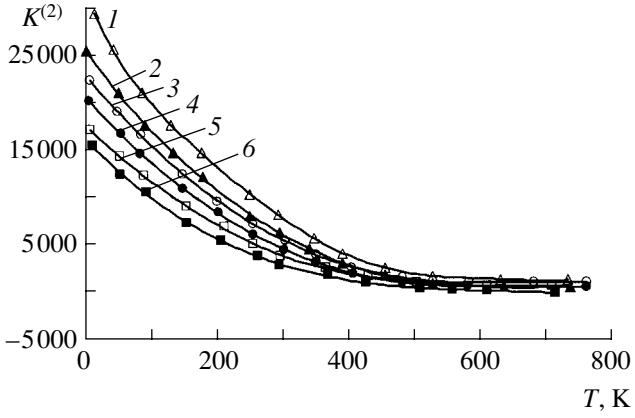

Fig. 10. Temperature dependence of $K^{(2)}$ for (*1*, *3*, *5*) longitudinal and (*2*, *4*, *6*) transverse strains in *p*-SOS ⟨110⟩-oriented piezoresistors. The hole density is (*1*, *2*) 2×10^{19}, (*3*, *4*) 6×10^{19}, or (*5*, *6*) 1.4×10^{20} cm^{-3}.

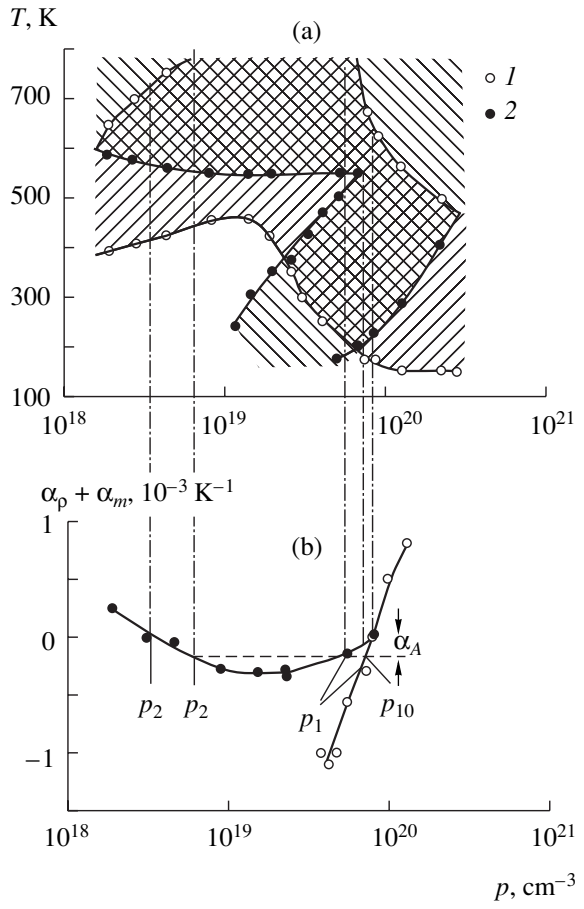

Fig. 11. Differential temperature invariance of piezoresistivity in *p*-SOS structures. In panel (a), the cross-hatched part is the region of temperature invariance and the boundaries of temperature invariance for α_ρ and α_m are indicated as (*1*) and (*2*), respectively. Panel (b) depicts the hole-density dependence of the sum $\alpha_\rho + \alpha_m$ in the region of temperature invariance, showing the temperature regions where Eq. (8) holds [12].

stant-voltage source producing I_E or U_E, respectively [25, 37]. Here, R_0 is the zero-input ($M = 0$) bridge resistance and the elastic coefficient K_s is defined by $\varepsilon = K_s(T)M$.

Let us first consider excitation by a constant-current source. Equation (5) implies that for the output to be temperature-independent the following condition must be fulfilled:

$$\alpha_R + \alpha_s + \alpha_m = 0, \tag{7}$$

where $\alpha_R = (dR(T)/dT)/R(T) \approx (d\rho(T)/dT)/\rho(T) = \alpha_\rho$ are the differential temperature coefficients of resistance and resistivity, respectively, and $\alpha_s = (dK_s(T)/dT)/K_s(T)$ is that of K_s. Note that α_s can be considered constant over a wide temperature range, so that Eq. (7) can be recast as

$$\alpha_\rho + \alpha_m = -\alpha_s \approx \text{const}. \tag{8}$$

It follows from Eqs. (1) and (4) that at suitable doping levels the sum $\alpha_\rho + \alpha_m$ is temperature-independent over a wide temperature range. This phenomenon is known as the differential-temperature invariance of piezoresistivity (DTIP) [11]; it is illustrated in Fig. 11a. Notice that the DTIP region consists of a low-temperature ($p \approx (0.27–3.0) \times 10^{20}$ cm^{-3}) and a high-temperature ($p \approx (0.15–7) \times 10^{19}$ cm^{-3}) part. Condition (8) can be fulfilled because α_ρ and α_m differ in sign. Figure 11b represents hole concentrations at which this is the case: p_{10} and p_{20} if $\alpha_s = 0$, p_1 for the low-temperature part, and p_1 and p_2 for the high-temperature part.

With respect to excitation by a constant-voltage source, Eq. (6) implies that the condition of temperature invariance has the form

$$\alpha_s + \alpha_m = 0. \tag{9}$$

Figure 9 shows that m_{44} is almost temperature-independent ($\alpha_m \approx 0$) at low temperatures and $p \geq 10^{20}$ cm^{-3}. α_s is small, so this stability against temperature variation yields the possibility of creating precision pressure transducers for cryogenic applications [40].

3. PROPERTIES OF NARROW *p*-SOS PIEZORESISTORS

In *p*-SOS sensing elements, piezoresistors are made as long and narrow mesas in contact with the substrate. They experience significant thermal stress as a result of thermal-expansion mismatch between silicon and sapphire.

More specifically a large shear stress arises on the upper surface of an SOS film owing to stress relaxation, especially on the sapphire/silicon/air contact line (Fig. 12). The shear stress decreases exponentially with increasing distance from the contact line in both the vertical and horizontal directions. Consequently, the

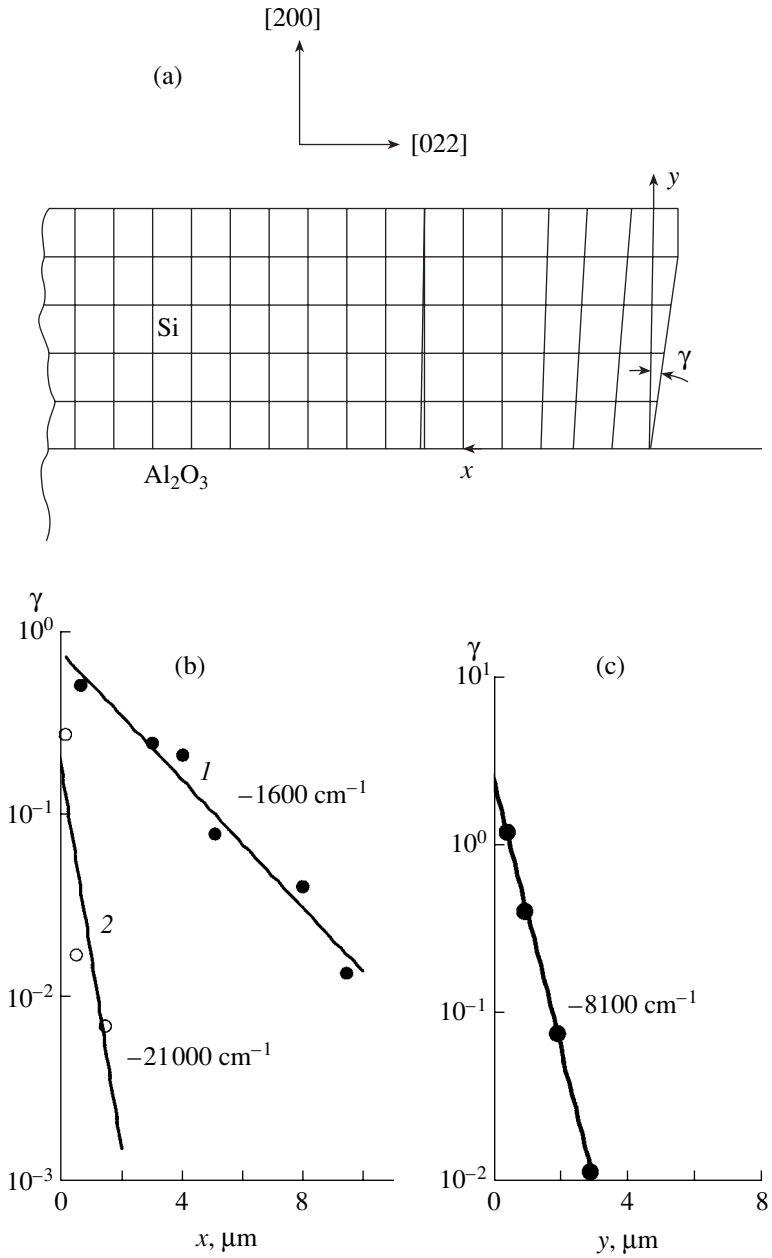

Fig. 12. Shear strain in SOS mesas [41]. Panel (a) illustrates how a shear strain $\varepsilon_\tau = \gamma$ arises at the edge of an SOS film, where γ is the deflection of the [200] direction from the normal to the [022] direction. Panel (b) shows γ vs. the planar distance to the edge of an SOS film (*1*) 7 or (*2*) 0.6 μm thick. Gradients *g* of the lines are equal to (*1*) –1600 and (*2*) –21000 cm^{-1}, with *g* defined by $\varepsilon_\tau = \varepsilon_{\tau 0}\exp(gx)$. Panel (c) shows *y* vs. distance *y* to the substrate for an SOS film 7 μm thick, the graph having a gradient of –8100 cm^{-1}.

mean thermal stress of a mesa will depend on whether the longitudinal or transverse direction is considered, so that resistivity ρ will vary with direction in a manner depending on the width-to-thickness ratio *b*/*d* (Fig. 13), a manifestation of the piezoresistive effect [42–44]. Close analytical approximations to experimental data have been constructed under the assumption that the longitudinal and transverse thermal strains in a resistor are given by $\varepsilon_{T\parallel} = \varepsilon_{T_0}$ and $\varepsilon_{T\perp} = \xi\varepsilon_{T_0}$ with $\xi \approx 1 - \exp(-0.11b/d)$, where ε_{T_0} is the strain in a homogeneous silicon film [42]. Calculations have revealed that the rate of change of ρ with *b*/*d* is maximal in ⟨110⟩-oriented resistors; this observation is in agreement with the measurements (Fig. 13b). For narrow resistors a change in resistivity is completely determined by the change in carrier mobility due to the piezoresistive effect [43].

The width-to-thickness ratio also influences α_ρ (Fig. 14) [25]. This dependence can also be approximated analytically to a sufficient accuracy under the

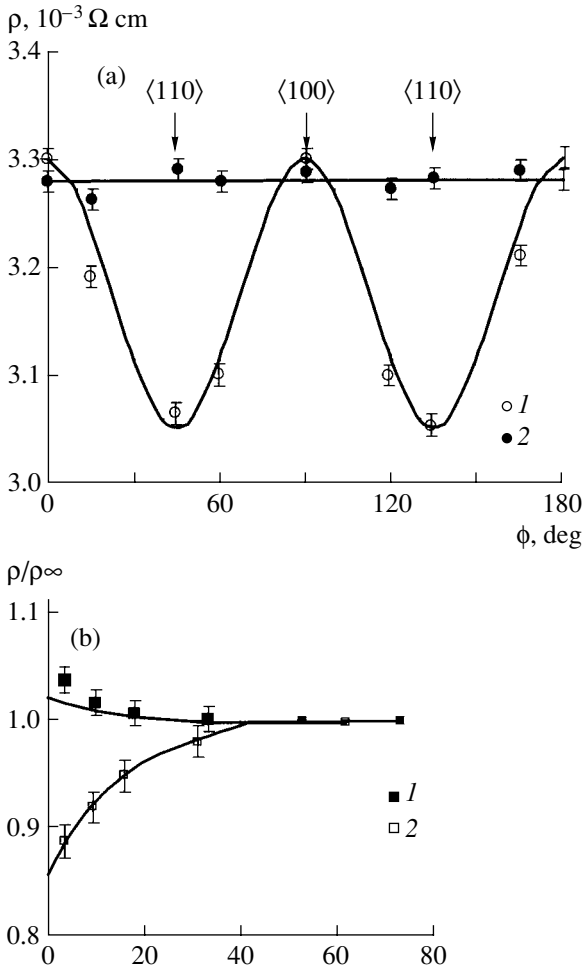

Fig. 13. Resistivity vs. (a) orientation or (b) width-to-thickness ratio in *p*-SOS piezoresistors. Panel (a) refers to resistors with $p = 4.8 \times 10^{19}$ cm^{-3} and b/d = (*1*) 9 and (*2*) 190. Panel (b) refers to resistors with p = (*1*) 4.3×10^{19} and (*2*) 5.4×10^{19} cm^{-3}, oriented along (*1*) ⟨100⟩ or (*2*) ⟨110⟩; the solid curves are for calculated values.

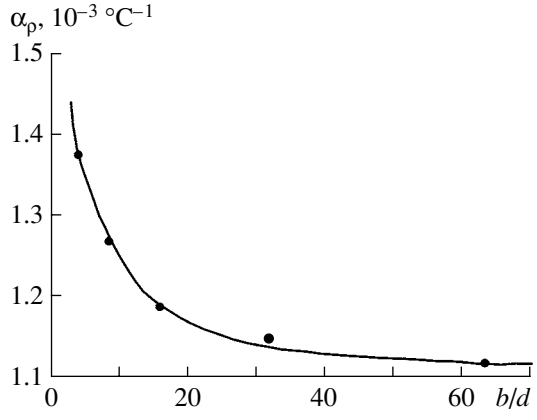

Fig. 14. Temperature coefficient of resistivity vs. width-to-thickness ratio at 250–450 K for narrow *p*-SOS resistors oriented as ⟨110⟩. The curve represents calculated values.

above assumption and in principle be used for temperature compensation of transducers [45], but this requires that SOS thickness and the width-to-thickness ratio be reproduced to an accuracy so high that it is almost unattainable by existing SOS technologies.

In mesa piezoresistors only the lower face is in contact with the substrate, with the result that the surface strain of a sensing element is transmitted into the bulk of the piezoresistors only partially (this is particularly true of the transverse direction), hence the dependence of $K^{(1)}$ and $K^{(2)}$ on b/d (Fig. 15) [46]. This property could be used for making the output of SOS transducers more linear.

Since $\alpha_R \approx \alpha_\rho$ and α_K depend on b/d, the sum $\alpha_\rho + \alpha_K$ (Fig. 16), as well as the optimal hole densities p_{10}, …, p_2, does also [25]. This fact should also be taken into account when designing the layout of a sensing element.

4. RADIATION EFFECTS ON SOS STRUCTURES

The high radiation hardness of SOS structures is of relevance to, for example, the design of pressure transducers for nuclear power plants. However, allowance must be made for the fact that neutron irradiation of heavily doped *p*-SOS structures significantly changes resistivity ρ, with hole concentration p and hole mobility μ affected to almost the same extent. Each of these three parameters as a function of the dose Φ closely obeys the phenomenological relation

$$x(\Phi)/x(0) \approx 1 + A(1 - \exp(-a\Phi)), \qquad (10)$$

where Φ is in the range $(0–3) \times 10^{17}$ cm^{-2} and parameters A and a depend on the original carrier concentration [47]. Similar behavior was observed in specimens subjected to gamma rays in a VVR-2000 reactor (Fig. 17) [48].

With Eqs. (5) and (6) in mind, we see that a *p*-SOS piezoresistive bridge excited by a constant-voltage source can tolerate large doses of neutrons or gamma rays, whereas one with a constant-current source cannot.

5. SOS PRESSURE TRANSDUCERS

5A. Transducer Designs

Sapphire can be rigidly joined to titanium and titanium alloys by brazing [49]. Therefore, in Russia SOS force and pressure transducers commonly employ a titanium-alloy diaphragm on which a sensing element is brazed [50]. Figure 18 is a schematic of pressure transducers designed at PG MIDA [10]. The designs in Figs. 18a–18c include a bilayered elastic element made from a titanium-alloy diaphragm and an SOS sensing element. Their advantages are high durability and reliability of the transducer; an easily adjustable dynamic range; possibility of making flush-mounted transduc-

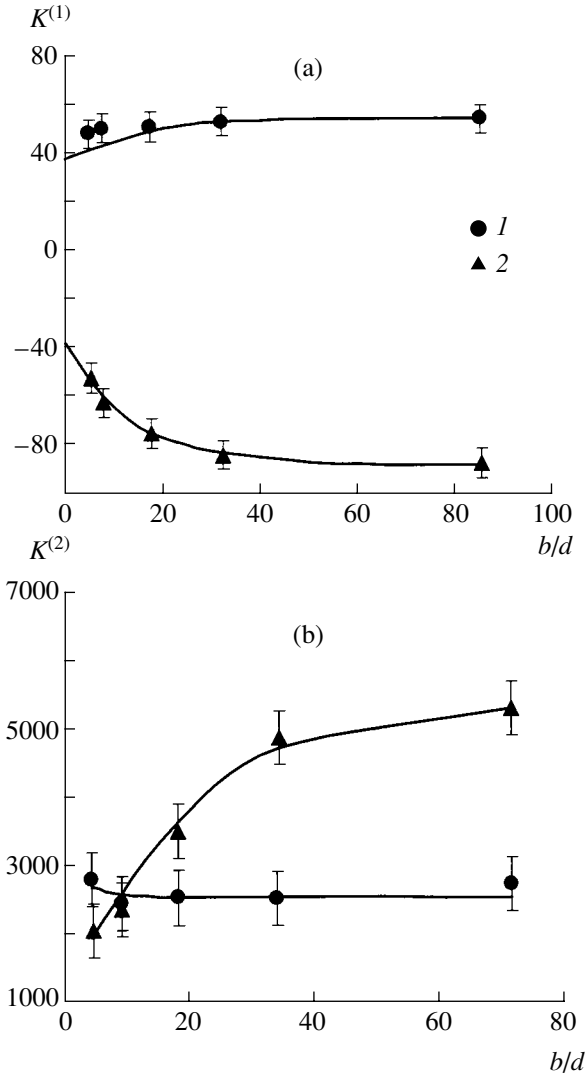

Fig. 15. Dependence of (a) $K^{(1)}$ and (b) $K^{(2)}$ on the width-to-thickness ratio for (*1*) longitudinal and (*2*) transverse *p*-SOS piezoresistors on a beam sensing element. The piezoresistors are ⟨110⟩-oriented, and $p \approx 5 \times 10^{19}$ cm^{-3}. The curves in panel (a) represent calculated values.

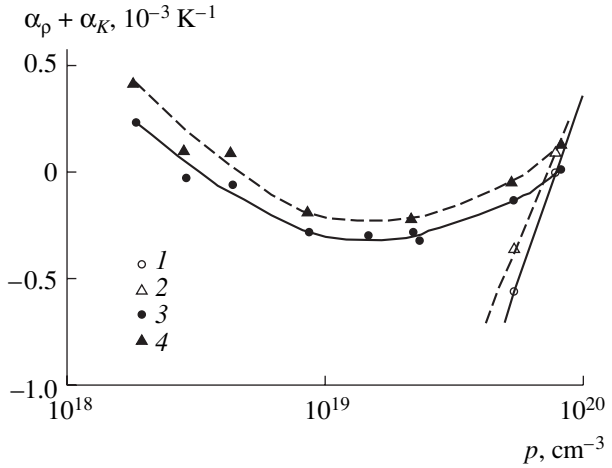

Fig. 16. Dependence of the sum $\alpha_\rho + \alpha_K$ on hole density for *p*-SOS piezoresistors with (*1*, *3*) $b/d \geq 60$ or (*2*, *4*) $b/d = 4$ to 8. Curves *1* and *2* correspond to a low-temperature part of the DTIP region; curves *3* and *4,* to a high-temperature part.

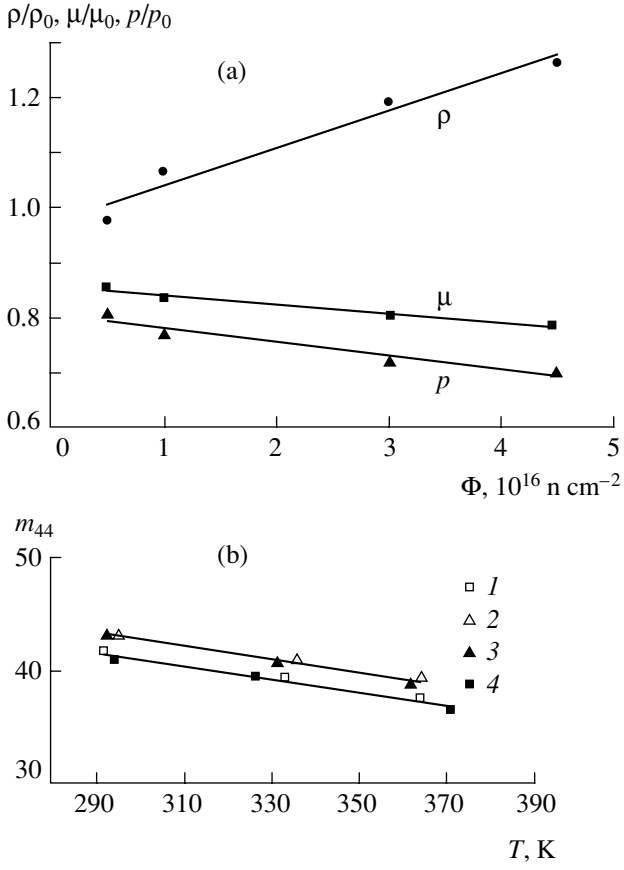

Fig. 17. (a) Dependence of the resistivity ρ, hole density *p*, and hole mobility μ on fluency of neutrons and (b) dependence of m_{44} on temperature for a *p*-SOS film irradiated in a reactor. Panel (a) is obtained at $T = 300$ K and $p_0 = 6 \times 10^{19}$ cm^{-3}. Panel (b) is obtained at $p_0 = 5 \times 10^{19}$ cm^{-3} and $\Phi =$ (*1*, *2*) 0, (*3*) 0.5×10^{16}, and (*4*) 4.5×10^{16} n cm^{-2}.

ers; and use of a unified, planar SOS element. The designs of Figs. 18b and 18c have a second diaphragm, to which external pressure is applied; the diaphragm can be made of a different material (such as stainless steel) suitable for use in corrosive media. On the other hand, the considerable thermal-expansion mismatch between titanium and sapphire leads to a higher thermal strain in the SOS sensing element and hence to a temperature effect on the offset in the piezoresistive bridge. Furthermore, the choice of titanium alloys is limited by the existing techniques of brazing.

In the design of Fig. 18d, the elastic diaphragm consists of the SOS sensing element itself. It is rigidly joined to an aluminosilicate-ceramic base by a high-melting solder glass, with the base made in the form of a ring or cup (for measuring differential or absolute

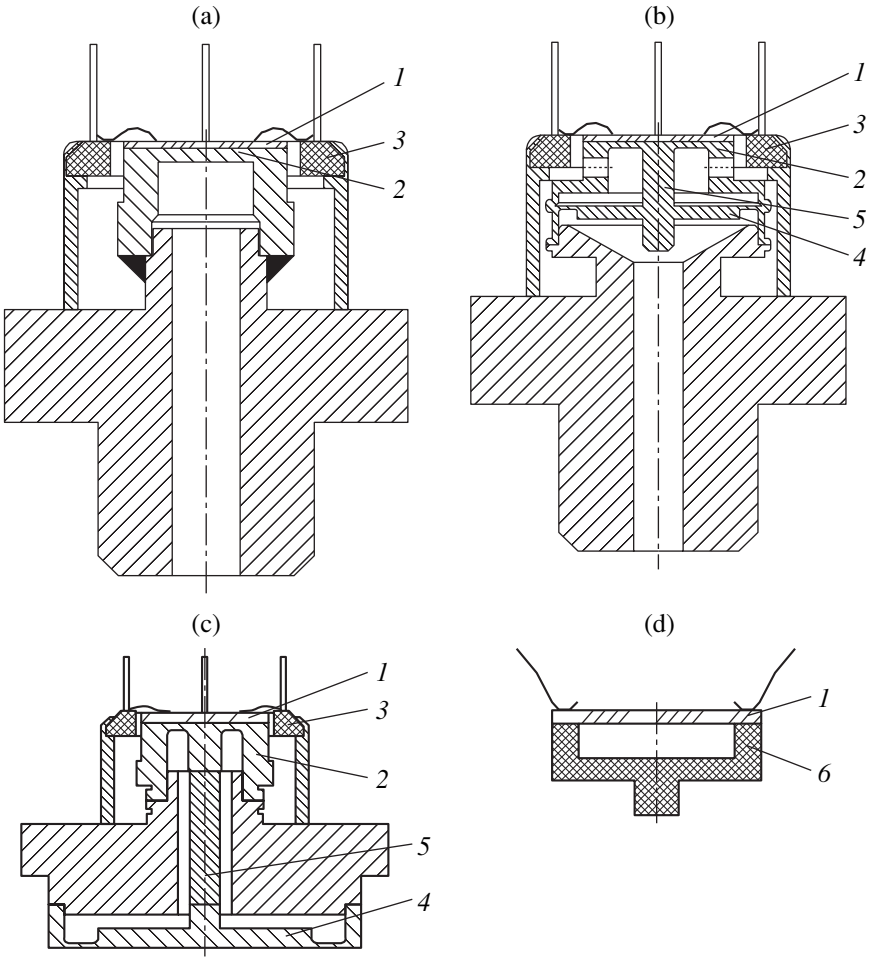

Fig. 18. Major designs of SOS pressure transducers (PG MIDA, Russia): (a, d) single- and (b, c) double-diaphragm designs including (*1*) an SOS sensing element, (*2*) an output metal diaphragm, (*3*) a collector, (*4*) an input metal diaphragm, (*5*) a rod, and (*6*) a ceramic base. Designs (a–c) are used for measuring differential pressure; design (d), for absolute pressure.

pressure, respectively). The temperature effect on the offset is thus reduced because aluminosilicate ceramic and $Al_2O_3(0112)$ have close coefficients of thermal expansion. On the other hand, changing the dynamic range necessitates replacing the sensing element with one of different thickness. Furthermore, a sufficiently linear output can be obtained only if pressure is applied to the piezoresistor side of SOS and the sapphire substrate has a suitable configuration [51]. Nevertheless, the design being considered has been successfully employed, e.g., in precision barometers.

Figure 19 shows a typical layout of an SOS sensing element for pressure transducers. A hard sapphire substrate allows manufacture of the sensing part of a piezoresistive transducer as a bridge circuit in the form of a closed loop and containing silicon balance resistors. This configuration eliminates the influence of the metal–silicon contact resistances, and the balance resistors and piezoresistors made from the same material make for higher temperature stability. Also important are the silicon doping level, the arrangement and shape of the piezoresistors (including the width-to-thickness ratio), and the shape of the area occupied by the piezoresistors [25]. Note that even a fairly large silicon area can experience thermal stress that is anisotropic and dependent on the shape of the area (Fig. 20).

Silicon-on-sapphire sensing elements use a homogeneous silicon film, and their layout (even a complex one) can be computed by Poisson's equation and the finite-element method. This approach allows one to reduce the bridge offset and to design balance resistors of given sensitivity [52].

In other countries SOS pressure transducers use a Ti–soldered-glass–sapphire elastic element [18] or a sapphire sensing element joined to a stainless-steel package [16].

5B. Accuracy of Piezoresistive Transducers

The main metrological characteristics of a piezoresistive transducer are the nonlinearity, hysteresis, and repeatability of transduction.

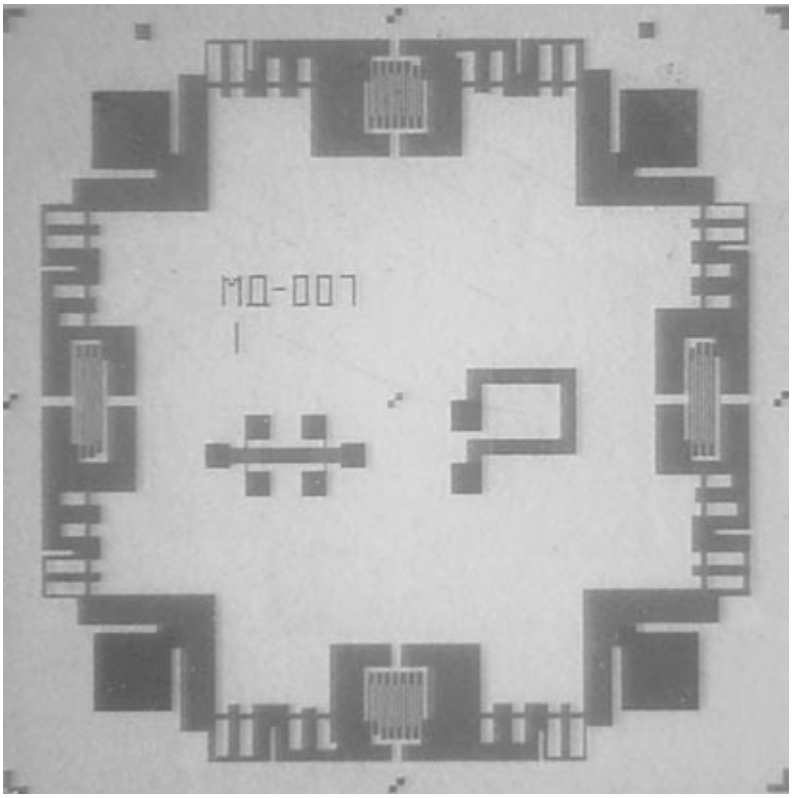

Fig. 19. Typical layout of an SOS sensing element for pressure transducers.

The nonlinearity depends on both the shape of the elastic element and the orientation of the piezoresistors relative to the direction of deformation (the former factor relates to mechanical conversion, whereas the latter, to transduction). Figure 21 depicts the temperature dependence of nonlinearity for a force transducer with a beam sensing element (having longitudinal and transverse piezoresistors) and for a pressure transducer with a diaphragm sensing element whose layout is shown in Fig. 19 [38]. It is seen that the nonlinearity of diaphragm transducers is almost flat over the range of possible operating temperatures. This allows employment of the same sensing element for cryogenic- and high-temperature applications. Figure 22a displays the mean value and dispersion of nonlinearity (at room temperature) for MIDA-DI-13P industrial pressure transmitters (Russia) with different pressure ranges. Notice that the output is linear to within 0.1% for an overwhelming majority of items.

Hysteresis and repeatability, unlike nonlinearity, cannot be improved by means of the electronic part of a transducer. Hysteresis can be reduced by using a sensing element of high crystalline quality, a highly elastic age-hardenable titanium alloy, and an inflexible solder (Fig. 22b). The repeatability of SOS pressure transducers can be better than 0.02–0.04% FS.

Foreign manufacturers claim to have improved the accuracy (the nonlinearity, hysteresis, and repeatability combined) to ±0.25% FS [16–18].

5C. Temperature Error

The error of the considered transducers is caused to a large extent by the temperature drift of the offset and sensitivity. In bilayered-diaphragm designs, the temperature drift of the offset mainly stems from thermal deformation of the SOS sensing element. Temperature drift of sensitivity results from temperature-induced variations in the resistance and sensitivity of the piezoresistive bridge (depending on the mode of excitation of bridge (5), (6)) and from the temperature dependence of the elastic coefficient K.

It is advantageous to reduce temperature drift by optimizing the design and fabrication process of transducers rather than by adjusting them individually. Examples are optimization of piezoresistor shape and arrangement and optimization of the silicon doping level. Regrettably this strategy cannot be implemented to the full extent at the current stage of SOS technology; therefore, different passive and active circuits are used to reduce temperature drift [54]. For example, designers at PG MIDA employ both passive circuits based on temperature-stable resistors [55] and digital signal processors. With temperature-stable resistors, it

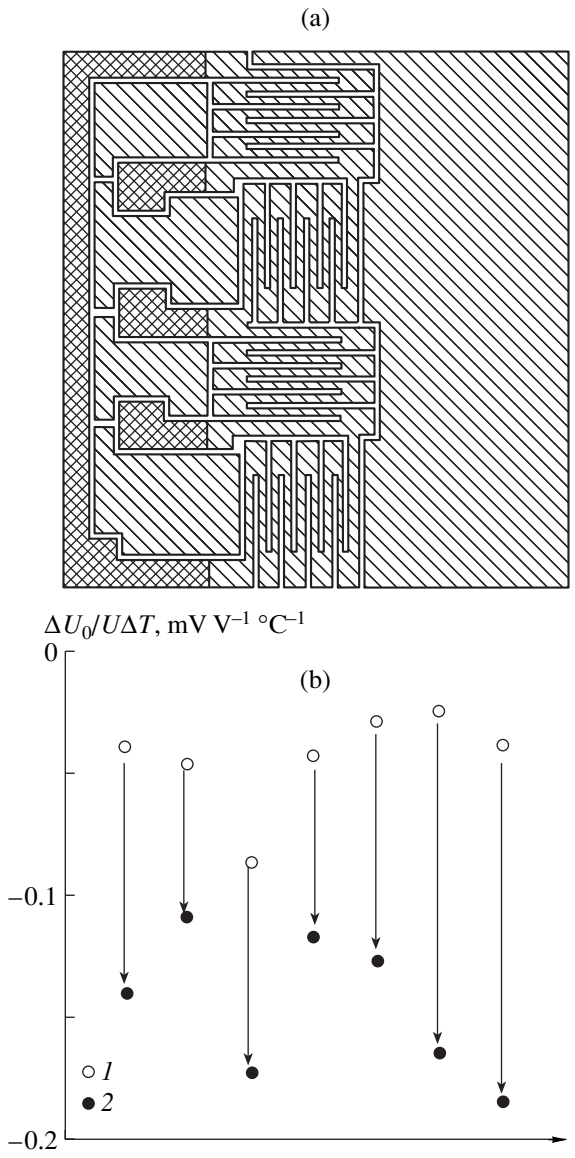

Fig. 20. Piezoresistive bridge circuit on a beam SOS sensing element with extra silicon areas: (a) layout and (b) graph of the temperature drift of the offset (*1*) with and (*2*) without the extra silicon areas for seven specimens.

is not necessary to ensure that the sensing element and compensation elements are at the same temperature and the temperature coefficients of compensation elements are irrelevant. Moreover, compensation elements can be placed on the transducer or its peripheral circuit board as is convenient; this advantage is especially important when pressure of a high-temperature medium is to be measured.

To suppress the temperature drift of the offset, a temperature-stable resistor can be connected in parallel with one arm of the piezoresistive bridge, and then the bridge is balanced with SOS resistors [55]. For a bridge using a constant-current source, this aim can be achieved using SOS balance resistors to set the offset to a calculated, temperature-independent value [56].

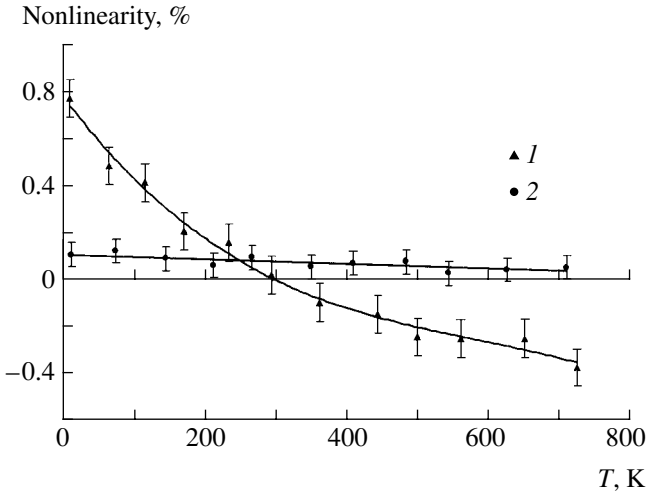

Fig. 21. Temperature dependence of nonlinearity for (*1*) a force transducer with a beam sensing element and (*2*) a pressure diaphragm transducer with a *p*-SOS sensing element.

Temperature drift of sensitivity can be suppressed by DTIP (see Eq. (7)). This approach is known as the self-compensation for temperature-induced variations in sensitivity and has been patented [57–60]. By way of illustration, Fig. 23 depicts different patterns of temperature drift of sensitivity depending on SOS resistivity [61]. Notice that the variation in sensitivity is within 1% over the temperature range –70 to 400°C if ρ = 2.6 mΩ cm; the sensitivity is almost temperature-independent over the range 200–400°C if ρ = 2.9 mΩ cm.

However, self-compensation suffers from two major drawbacks. First, if the resistivity deviates from an optimal value by a mere 10%, the temperature drift of sensitivity will increase dramatically (Fig. 23), and it is not feasible to achieve a better accuracy by existing doping techniques for *p*-SOS films. Second, the optimal value of resistivity depends on α_s, which is determined by both the material and the design of the transducer. Consequently, optimal resistivity is generally specific to the design of a transducer and its dynamic range. For practical purposes the temperature drift of sensitivity in a transducer using a constant-current source is suppressed by doping the *p*-SOS film to a level somewhat higher than the optimum, with the residual drift compensated for by connecting a temperature-stable resistor in parallel with the bridge circuit excited by a current source [55].

If a pressure transducer requires employment of a constant-voltage source, as is often the case, it is again advantageous to use a *p*-SOS film of an elevated doping level, which reduces the temperature coefficient of the gage factor. In this case a temperature-stable resistor should be connected in series with the source of excitation [55].

It is important to note that both the offset and the sensitivity of a transducer vary in a nonlinear manner with temperature in most cases because of the nonlinear behavior of the sensing element. For example, the respective temperature drifts of offset and sensitivity in SOS pressure transducers using temperature-stable resistors for compensation follow a pattern approximating a parabola (Fig. 24). For this reason it is usually not appropriate to characterize the temperature drift in transducers in terms of the first derivative with respect to temperature [16–18, 62]. Instead one should use the range of the extra temperature drift with respect to an operating temperature range when specifying the allowable temperature drift [63]. Figure 25 represents the ranges of the extra temperature drift for MIDA-13P pressure transmitters with different pressure ranges; the drift data refer to the SOS transducer and the electronic unit combined [53].

Figure 26 displays the distributions of the ranges of the overall temperature drift over samples of MIDA-01P or MIDA-13P. In these models the piezoresistive bridges are designed to be excited by a constant-current or constant-voltage source, respectively, with compensation provided by temperature-stable resistors. It is seen that the extra temperature drift can thus be reduced to a fairly small amount, which is almost the same for both modes of excitation.

Since temperature dependence of the transducer output can be approximated by a parabola, it is easy to employ digital signal processing to compensate for the temperature drift. With MIDA-13P-K transducers, the overall measurement error can thus be decreased to below 0.25% in the temperature range −40 to 80°C (Fig. 27) [53].

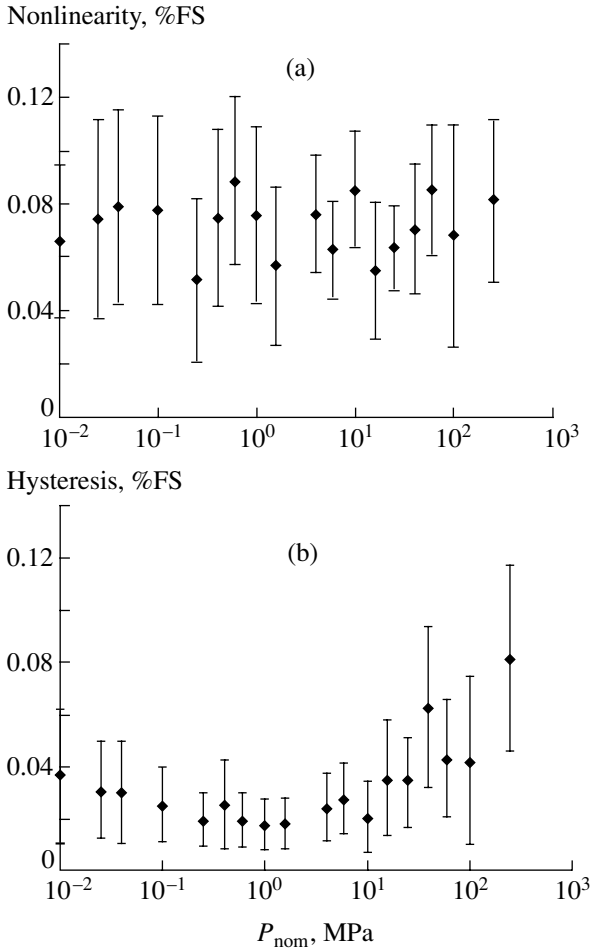

Fig. 22. Mean value and dispersion of (a) linearity and (b) hysteresis for MIDA-DI-13P pressure transmitters differing in dynamic range (sample size 15000) [53].

5D. Stability

Stable performance is a major requirement placed on transducers, particularly on those intended for applications where regular calibration is laborious or impossible (as in nuclear reactors, spacecraft, etc.). On the other hand, stability is the most difficult characteristic to define because it depends crucially on operating conditions. For example, it is clear that three different pressure transducers which are being kept in storage, operated indoors at a constant pressure, and operated outdoors at a rapidly changing pressure, respectively, will show entirely different patterns of variation in performance over a year. Regrettably most manufacturers fail to specify the operating conditions under which the stability of their products have been evaluated.

It is established practice at PG MIDA to regularly test the stability of piezoresistive pressure transducers by temperature cycling over the operating range because temperature variations are known to be a major factor affecting their performance. Below we present typical variations in the main metrological characteristics, expressed in percent of the full scale, as observed

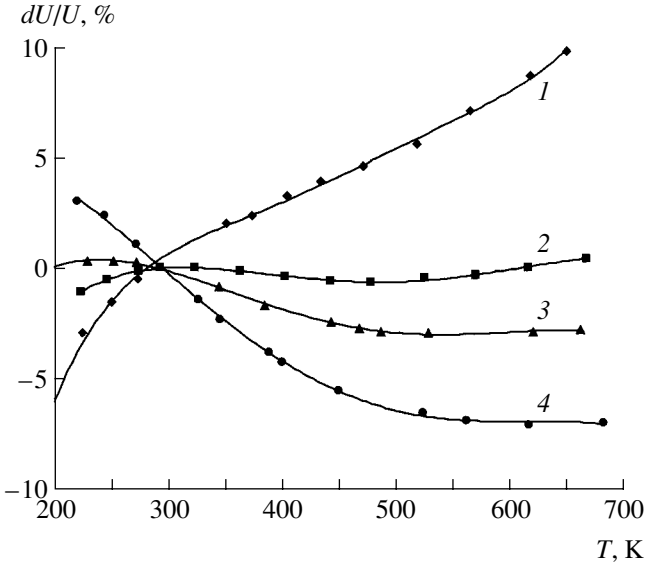

Fig. 23. Percentage change in sensitivity vs. temperature for pressure transducers with a bilayered diaphragm elastic element. The silicon resistivity is (*1*) 2.3, (*2*) 2.6, (*3*) 2.9, or (*4*) 3.8 mΩ cm.

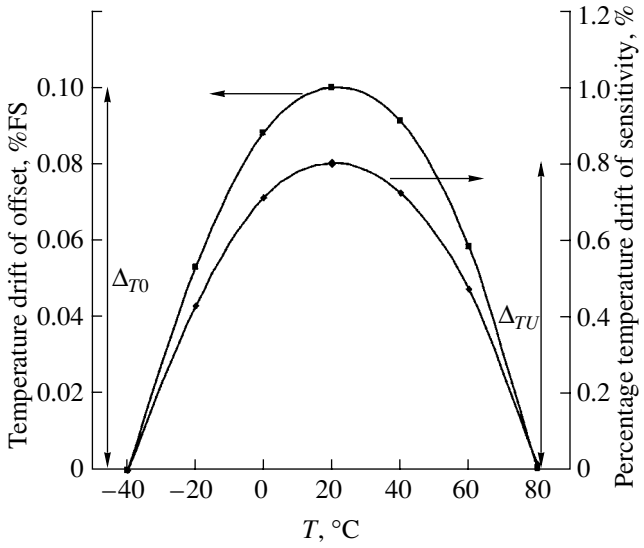

Fig. 24. Typical patterns of the temperature drift of the offset and sensitivity in SOS pressure transducers using temperature-stable resistors for compensation, with excitation provided by a constant-voltage source. The curves are parabolas. The respective ranges of the temperature drift for the offset and sensitivity are denoted Δ_{T0} and Δ_{TU}.

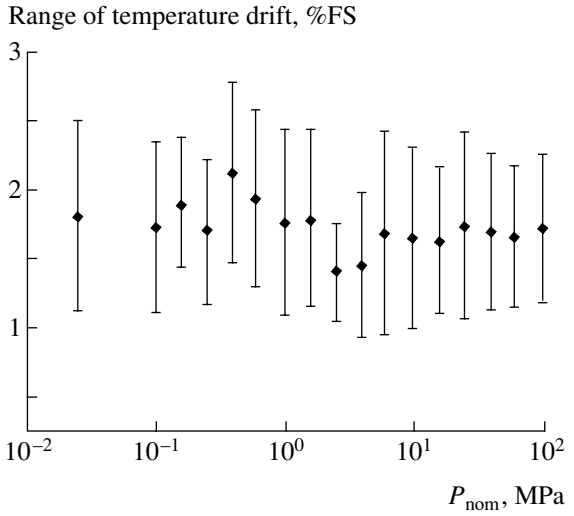

Fig. 25. Mean value and dispersion of the temperature drift at different operating pressures for MIDA-DI-13P transmitters with different pressure ranges, the temperature varying from –40 to 80°C. The drift data refer to the transducer and the electronic unit combined.

in a test of 250 temperature cycles over the range –40 to 80°C.

Offset: ±0.1
Sensitivity: ±0.05
Nonlinearity: ±0.03
Hysteresis: ±0.02
Repeatability: ±0.03
Accuracy: ±0.05

Notice that the offset is the least stable, whereas the sensitivity and accuracy (i.e., the nonlinearity, hysteresis, and repeatability combined) are almost unaffected by the temperature cycles.

5E. High-Temperature Operation

A major advantage of SOS transducers is that they can operate at high temperatures. Theoretically, SOS films can withstand temperatures reaching 600–700°C, as determined by the onset of appreciable plastic deformation of the silicon [64]. However, the allowable temperatures of most SOS transducers available do not exceed 400°C owing to process limitations [16]. For example, MIDA-DI-12P-12 can be operated at up to 350°C, its sensing element working at the temperature of the medium under measurement [10].

The maximum operating temperature can be substantially increased by changing to a flush-mounted, double-diaphragm design because this greatly reduces the temperature of the sensing element relative to the temperature of the medium. For example, the maximum operating temperature of the MIDA-DI-55P pressure transducer lies in the range 500–600°C, yet the temperature of its sensing element remains within 250°C (MIDA-DI-55P is designed for use in the cylinders of high-powered diesel engines). Flush-mounted transducers can measure pressure of viscous or crystallizable media, such as melted plastics. In Dynisco's transducers melt pressure is transmitted over a mercury-filled capillary tube to a pressure transducer working at room temperature [65]. By contrast MIDA-DI-12P-083 employs a rod to transmit applied pressure between two diaphragms (Fig. 16c). With the mercury removed, the transducer is environmentally safe and is suitable for the food and pharmaceutical industries.

Since temperature remains within a narrow range during most high-temperature manufacturing processes, MIDA-12P transducers are calibrated at the operating temperature. This eliminates the temperature drift due to heating of the medium from room to operating temperature. The extra temperature drift associated with a 100°C range around the calibration temperature is compensated for with temperature-stable resistors located in a zone of moderate temperature. As a result, the accuracy of high-temperature pressure transducers is within 0.2–0.5% and the extra temperature error is within 3%.

5F. Cryogenic-Temperature Operation

With cryogenic fluids, pressure measurement is faced with the issues of (i) how to transmit applied pressure to a zone of moderate temperature in which it can be measured with ordinary transducers and (ii) how to compensate for serious pressure variations arising in this zone [40]. Investigations of the piezoresistive effect in SOS structures have revealed that it is possible to create SOS transducers for temperatures down to the liq-

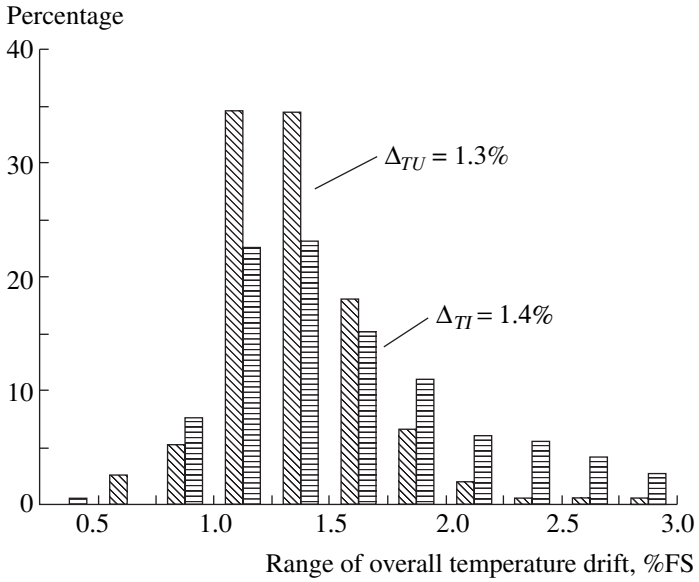

Fig. 26. Distributions of ranges of the overall temperature drift over samples of MIDA-01P or MIDA-13P transducers (using constant-current or constant-voltage excitation, respectively), the temperature varying from –40 to 80°C [55].

uid-helium temperature [66]. Indeed, prototype transducers were fabricated that showed impressive performance: nonlinearity of better than 0.3% over the range 2–300 K and hysteresis within 0.1% [67]. Furthermore, the magnetic-field sensitivity was less than 0.05% T^{-1}, and the magnetic-field response was linear for fields up to 9 T [67]. With a *p*-SOS film of optimal resistivity and constant-voltage-source excitation, pressure transducers were obtained whose sensitivity is flat within 0.2% over the temperature range 2–77 K or within 4% over the range 2–300 K (Fig. 28).

6. PROSPECTIVE DEVELOPMENTS

The performance of SOS transducers continues to improve. For example, early designs, such as the Sapfir-22 pressure transmitters, were unable to provide an accuracy better than 0.25% and diaphragm pressure transducers were unsuitable for use below 100 kPa (for lower pressures the elastic diaphragm connected to a force transducer was used); now we have MIDA-13P industrial pressure transmitters accurate to within 0.1% and diaphragm transducers for pressures down to 4 kPa.

We see a number of directions in which SOS transducers may be developed. First, mathematical models are desirable that would enable optimization of the structure of the transduction element and the layout of the piezoresistive bridge. For example, it has been revealed that the surface deformation of the diaphragm in a piezoresistive transducer is transmitted beyond the boundary of the diaphragm; in fact, maximum sensitivity is achieved by placing the piezoresistors outside the diaphragm if the latter is sufficiently thick [68]. However, an accurate mathematical model has yet to be constructed that describes the surface deformation of a thick multilayered diaphragm by an applied pressure, with the diaphragm and its base made as an integral unit. Nor do we have a model of the stress arising on a sapphire substrate after brazing due to the thermal-expansion mismatch between sapphire and titanium. One of the reasons for this is that incorporating the anisotropy of mechanical properties of sapphire into a mathematical model is no easy task [69].

Second, in principle, the operating temperature of an SOS transducer can be raised to 500–600°C, whereas the present-day operating temperature does not exceed 350–400°C. However, this would necessitate making ohmic contacts to silicon suitable for such high temperatures. How to accomplish this remains an open question.

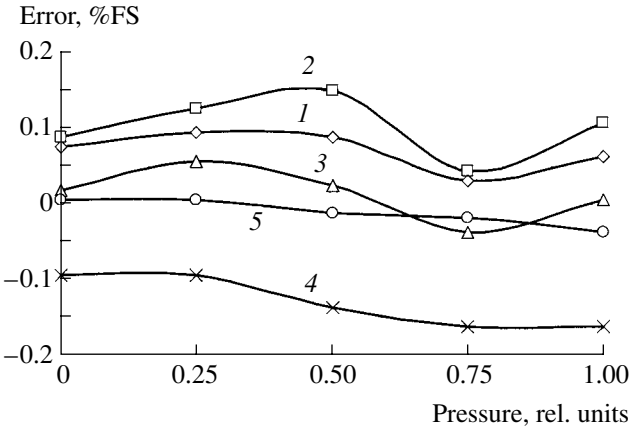

Fig. 27. Measurement error vs. applied pressure for a MIDA-DI-13P-K transmitter at temperatures of (*1*) –40, (*2*) –20, (*3*) 20, (*4*) 50, and (*5*) 80°C. The pressure is normalized to its maximum value.

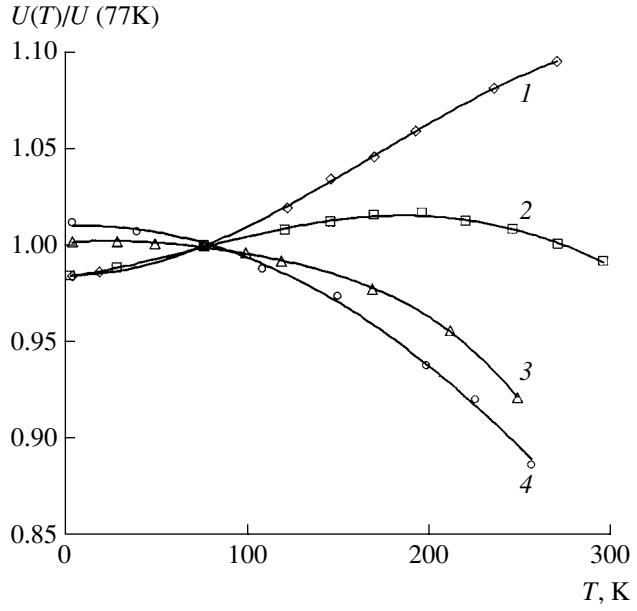

Fig. 28. Temperature dependence of sensitivity subject to the SOS doping level in pressure transducers for cryogenic applications: p = (*1*) 2.4×10^{20}, (*2*) 1.4×10^{20}, (*3*) 7.2×10^{19}, (*4*) 6×10^{19} cm^{-3} [12, 67].

Third, it is of great interest to create pressure transducers for cryogenic-temperature operation. Although this goal has long been known as achievable in principle, cryogenic transducers are still in the research and development stage.

Fourth, note that titanium or its alloys cannot be used for measurements in highly corrosive media such as oxygen or hydrogen. Double-diaphragm designs with an input diaphragm made from stainless steel, for example, can serve this purpose. However, this approach is faced with the problem of reliable joining of stainless steel and a titanium alloy together while ensuring the resilient behavior of the resulting structure.

These are some directions of development that may lead to many new uses of SOS structures in mechanical transducers.

REFERENCES

1. V. S. Papkov and M. B. Tsybul'nikov, *Epitaxial Silicon Layers on Insulating Substrates and Their Applications* (Energiya, Moscow, 1979) [in Russian].
2. NPP Sapfir, http://www.sapfir.ru/science.htm.
3. Dynex Semiconductor, http://www.dynex-semi.com/products/sos/index.htm.
4. A. G. Andreou, Z. K. Kalayjian, A. Apsel, *et al.*, IEEE Circuits Syst. Mag. **1** (3), 22 (2001).
5. M. E. Ksenofontov, Prib. Sist. Upr., No. 3, 61 (1970).
6. M. E. Ksenofontov and M. V. Surovikov, Prib. Tochnoi Mekh. Tekhnol. Priborostr., No. 2, 176 (1972).
7. V. L. Kenigsberg, V. I. Serdyukov, S. I. Mil'man, *et al.*, Prib. Sist. Upr., No. 7, 26 (1974).
8. V. L. Kenigsberg, V. M. Stuchebnikov, V. I. Serdyukov, *et al.*, Izmer. Tekh., No. 10, 84 (1978).
9. G. G. Iordan, in *Microelectronic Transducers for Measuring Mechanical and Thermal Properties* (MDNTP, Moscow, 1980), p. 3 [in Russian].
10. V. V. Bushev, O. L. Nikolaichuk, and V. M. Stuchebnikov, Datchiki Sist., No. 1, 21 (2000).
11. V. M. Stuchebnikov, Izmer. Kontrol. Avtom., No. 4, 15 (1982).
12. V. M. Stuchebnikov, Sens. Actuators A **28**, 207 (1991).
13. O. P. Perepelitsyn and S. V. Blagodetelev, Datchiki Sist., No. 10, 20 (2002).
14. Datchiki Sist., No. 10, 46 (2003).
15. L. N. Kolomiets, Datchiki Sist., No. 10, 44 (2001).
16. Sensonetics, Inc., Silicon on Sapphire Pressure Transducers, http://www.sensonetics.com/series400.pdf.
17. Pressure Sensors, http://www.eldec.com/pressure_sensors.htm.
18. PX4200-5V: Silicon on Sapphire Pressure Transducer, Outstanding Performance and Stability, http://www.omega.com/pptst/PX4200-5V.html.
19. A. M. Manasevit, J. Cryst. Growth **22**, 125 (1974).
20. B. I. Pivonenkov and V. M. Stuchebnikov, Prib. Sist. Upr., No. 1, 20 (1976).
21. J. E. A. Mauritis, Solid State Technol. **20** (4), 81 (1977).
22. V. M. Stuchebnikov, Obz. Elektron. Tekh., Ser. 6: Materialy, No. 2 (1980).
23. V. M. Stuchebnikov and V. S. Papkov, Elektron. Prom–st., No. 8, 71 (1980).
24. M. S. Abrahams and C. J. Buiocchi, Appl. Phys. Lett. **27**, 325 (1975).
25. V. M. Stuchebnikov, Doctoral Dissertation in Technical Sciences (NIITeplopribor, Moscow, 1986).
26. D. J. Dumin and P. H. Robinson, J. Appl. Phys. **39**, 2759 (1968).
27. W. R. Thurber, R. L. Mattis, and Y. M. Liu, in *Semiconductor Characterization Techniques: Proceedings of the Topical Conference on Characterization Techniques for Semiconductor Materials and Devices, Seattle, Wash., Princeton, N.J., 1978*, p. 81.
28. W. R. Thurber, R. L. Mattis, and Y. M. Liu, J. Electrochem. Soc. **127**, 2291 (1980).
29. D. N. Dutta, Phys. Status Solidi **2**, 984 (1962).
30. K. G. Lyon, G. L. Salinger, C. A. Swenson, and G. K. White, J. Appl. Phys. **48**, 865 (1977).
31. J. B. Watchman, Jr., T. G. Scuderi, and G. W. Cleek, J. Am. Ceram. Soc. **45**, 319 (1962).
32. D. M. Jefkins, J. Phys. D: Appl. Phys. **3**, 770 (1970).
33. D. J. Dumin, J. Appl. Phys. **36**, 2700 (1965).
34. V. S. Papkov and N. S. Papkov, Elektron. Tekh., Ser. Materialy, No. 7, 67 (1977).
35. V. M. Stuchebnikov, V. I. Sukhanov, and V. V. Khasikov, Prib. Sist. Upr., No. 1, 83 (1983).

36. G. I. Lur'e and V. M. Stuchebnikov, Elektron. Tekh., Ser. Materialy, No. 1, 16 (1984).
37. G. I. Lur'e, V. M. Stuchebnikov, and V. I. Sukhanov, in *Theoretical and Experimental Research on the Design of Semiconductor Measuring Transducers* (NIITeplopribor, Moscow, 1986), p. 3 [in Russian].
38. G. I. Lur'e, V. M. Stuchebnikov, and V. I. Sukhanov, in *Theoretical and Experimental Research on the Design of Semiconductor Measuring Transducers* (NIITeplopribor, Moscow, 1986), p. 15 [in Russian].
39. L. B. Wilner, ISA Trans. **17** (1), 83 (1978).
40. G. I. Lur'e and V. M. Stuchebnikov, Izmer. Kontrol. Avtom., No. 2, 18 (1989).
41. M. S. Abrahams, J. Blanc, C. J. Buiocchi, and W. E. Yfm, J. Appl. Phys. **49**, 652 (1978).
42. V. M. Stuchebnikov, Prib. Sist. Upr., No. 6, 26 (1982).
43. A. V. Beloglazov, V. M. Stuchebnikov, V. V. Khasikov, and V. N. Chernitsyn, Fiz. Tekh. Poluprovodn. (Leningrad) **16**, 1483 (1982).
44. V. M. Stuchebnikov and V. N. Chernitsyn, in *Theoretical and Experimental Research into Novel Measuring Transducers and Topics in Computer-Aided Design* (NIITeplopribor, Moscow, 1985), p. 3 [in Russian].
45. V. I. Evdokimov, V. M. Stuchebnikov, V. I. Sukhanov, *et al.*, SU Inventor's Certificate No. 1,404,850, Byull. Izobret., No. 23 (1988).
46. A. A. Beloglazov, I. K. Lazareva, V. M. Stuchebnikov, and V. I. Sukhanov, Prib. Sist. Upr., No. 8, 30 (1982).
47. B. V. Koba, V. L. Litvinov, A. L. Ocheretyanskii, *et al.*, Fiz. Tekh. Poluprovodn. (Leningrad) **19**, 1017 (1985).
48. B. V. Koba, V. L. Litvinov, A. L. Ocheretyanskii, *et al.*, At. Energ. **59**, 58 (1985).
49. Z. V. Nikiforova, S. G. Rumyantsev, S. L. Kiselevskii, and V. I. Evdokimov, Svar. Proizvod., No. 3, 35 (1974).
50. A. V. Beloglazov, V. M. Stuchebnikov, V. V. Khasikov, *et al.*, Prib. Sist. Upr., No. 5, 21 (1982).
51. N. S. Papkov, V. S. Papkov, and V. M. Stuchebnikov, Datchiki Sist., No. 5, 30 (1999).
52. A. V. Pirogov and V. M. Stuchebnikov, in *Issues of Automation and Control of Engineering Systems: Proceedings of International Conference, Penza, Russia, 2004* (IITsPGU, Penza, 2004), p. 113.
53. E. E. Bushev, O. L. Nikolaichuk, and V. M. Stuchebnikov, Datchiki Sist., No. 6, 48 (2004).
54. V. I. Vaganov, *Integrated Piezoresistive Transducers* (Energoatomizdat, Moscow, 1983) [in Russian].
55. D. B. Martynov and V. M. Stuchebnikov, Datchiki Sist., No. 10, 6 (2002).
56. G. I. Lur'e, V. M. Stuchebnikov, V. I. Sukhanov, and D. A. Yachuk, SU Inventor's Certificate No. 1411571, Byull. Izobret., No. 27 (1988).
57. A. V. Beloglazov, V. E. Beiden, G. G. Iordan, *et al.*, SU Inventor's Certificate No. 934257, Byull. Izobret., No. 21 (1982).
58. US Patent No. 4,373,399 (1983).
59. FR Patent No. 8,027,919 (1983).
60. GDR Patent No. 156,488 (1982).
61. V. M. Stuchebnikov, in *Transducers for Measurement, Monitoring, and Control* (Penza Polytechnical Institute, Penza, 1985), p. 18 [in Russian].
62. *GOST* (National Standard) *22520-85 (ST SEV 4124-83): Pressure, Negative-Pressure, and Differential-Pressure Transducers with Analog Electrical Output: General Specifications.*
63. V. M. Stuchebnikov, Datchiki Sist., No. 9, 15 (2004).
64. Yu. A. Kontsevoi, Yu. M. Litvinov, and E. A. Fattakhov, *Plasticity and Strength of Semiconductor Materials and Structures* (Radio i Svyaz', Moscow, 1982) [in Russian].
65. Dynisco: Your Melt Pressure Transducer, http://www.dynisco.com.
66. G. I. Lur'e, V. M. Stuchebnikov, and V. V. Khasikov, Prib. Sist. Upr., No. 9, 20 (1981).
67. V. I. Evdokimov, G. I. Lur'e, and V. M. Stuchebnikov, Prib. Sist. Upr., No. 5, 19 (1985).
68. A. V. Beloglazov, V. I. Evdokimov, E. B. Kotlyarevskaya, *et al.*, SU Inventor's Certificate No. 1,525,505, Byull. Izobret., No. 44 (1989).
69. V. M. Stuchebnikov, Prib. Sist. Upr., No. 6, 40 (1983).